Journal of Materials Chemistry B

ROYAL SOCIETY OF CHEMISTRY

PAPER

View Article Online
View Journal

Cite this: DOI: 10.1039/d6tb00152a

Impact of phospholipase A_2 hydrolysis on triplet–triplet annihilation upconversion liposomes

Amrutha Prabhakaran, † Nirod Kumar Sarangi, † Colm Smith, Ruben Arturo Arellano Reyes and Tia E. Keyes *

Triplet–triplet annihilation upconversion (TTA-UC) liposomes are of emerging interest because of their potential bioapplications in biosensing/imaging and light-driven therapeutic delivery. However, a potential challenge *in vivo* is their stability, since liposomes are prone to enzymatic degradation. Here, for the first time, we examine the impact of phospholipase hydrolysis on TTA-UC in liposomes. We applied a TTA-UC liposome integrating a BODIPY charge transfer sensitizer and perylene emitter pair within a DOPC membrane, that exhibits intense upconverted blue emission under green excitation. Phospholipase A_2 (PLA_2) enzyme was applied as the phospholipase as it is ubiquitous in the body and upregulated under a number of conditions. Surprisingly, we observed that PLA_2 treatment resulted in only a relatively modest decrease in TTA-UC intensity on exposure of the liposomes to the enzyme. In the presence of imipramine, a competitive inhibitor of PLA_2, or absence of Ca^{2+} on which phospholipase hydrolysis depends, the enzymatic action is inhibited and TTA-UC intensity is indistinguishable from that in enzyme-free solution. Ca^{2+}-dependent enzymatic activity, drug-based inhibition and the impact of hydrolytic products on membrane packing were characterized in pore-suspended lipid bilayers, using confocal-based fluorescence lifetime imaging (FLIM), fluorescence lifetime correlation spectroscopy (FLCS), and electrochemical impedance spectroscopy (EIS). FLIM and FLCS studies show that enzymatic lipid cleavage increases lipid packing and decreases membrane fluidity without significant damage to the bilayer. Thus, we conclude that the decreased TTA-UC output is due to the increased viscosity of the membrane upon hydrolysis. Electrochemcial impedance confirms these observations, where membrane admittance decreases in response to phospholipid hydrolysis indicating tighter lipid packing of the membrane with hydrolytic products. Nanoscale imaging, using atomic force microscopy (AFM) in liquid mode at a mica-supported lipid bilayer, further confirmed that PLA_2 causes phospholipid hydrolysis in the presence of Ca^{2+}, resulting in nanoscale pore formation, whereas either in the absence of Ca^{2+} or with imipramine-treated PLA_2, it did not induce lipid hydrolysis. Overall, our findings provide a molecular basis for understanding enzymatic action in general at a liposome bilayer model and show, for the first time, the influence of enzyme hydrolysis on TTA-UC integrity and efficiency in liposomes.

Received 19th January 2026,
Accepted 28th May 2026

DOI: 10.1039/d6tb00152a

rsc.li/materials-b

1. Introduction

Triplet–triplet annihilation upconversion (TTA-UC) is a photophysical process in which two triplet sensitizer molecules, excited by low-energy (long-wavelength) light, transfer energy to triplet acceptor molecules. Upon mutual collision, the excited acceptors then undergo an annihilation reaction, promoting one molecule to the excited singlet state while the other relaxes to the ground state.[1–5] This excited acceptor fluoresces, emitting a photon at a higher frequency (higher energy) than that of the excitation originally used to initiate the process.[6–9]

TTA-UC is gaining traction as a route to light-induced activation in processes such as photoactivated drug release and bioimaging, because it offers the opportunity to use long wavelength, tissue-penetrating light to generate higher energy photons locally.[10–13] A promising approach to applying TTA-UC *in vivo* is *via* encapsulation of the dye system within liposomes. Liposomes are not only biocompatible drug delivery vehicles but also an effective scaffold for TTA-UC. This is because by confining the dyes to the two-dimensional (2D) space of the lipid bilayer, liposomes lead to increased collision probability that can significantly boost upconversion efficiency, depending on the conditions.[5,14]

A number of TTA-UC liposomal systems have been reported. For example, Askes *et al.* used a palladium tetraphenyltetrabenzoporphyrin complex as the photosensitizer and perylene as

School of Chemical Sciences and National Centre for Sensor Research, Dublin City University, Dublin 9, Ireland. E-mail: tia.keyes@dcu.ie
† These authors contributed equally to this work.

the annihilator within giant unilamellar vesicles (GUVs) composed of either DOPC or DMPC to image membranes under red-to-blue light upconversion.[15] Exploiting large unilamellar vesicles (100 nm diameter) of DOPC, DMPC, DSPC, *etc.* Poznik *et al.* studied TTA-UC in liposomes incorporating platinum porphyrin PtOEP and an amphiphilic derivative of tris-(bipyridine) ruthenium(II) as photosensitizers and lipophilic diphenylanthracene as the annihilator.[16] The reconstitution and selection of membrane composition and its intrinsic fluidity are as important for efficient TTA-UC as sensitizer–annihilator selection. Recently, we reported that a more fluidic liposomal membrane (low viscosity environment) leads to more efficient TTA-UC than a high viscosity membrane due to a higher probability of collision between the sensitizer and annihilator, which is crucial when designing a model for bioimaging.[5] We also demonstrated that the relative orientation of the sensitizer and annihilator (B2PI–perylene) within the lipid bilayer is a critical factor for efficient TTA-UC.[14]

Overall, therefore, liposomal TTA-UC is now well established; however, for most reported systems, *in vivo*/*vitro* biological applications are the ultimate aim, and, an important consideration that has not been addressed to date, is if enzymatic activity impacts TTA-UC within such systems.[5] The cellular environment contains endogenous enzymes that target phospholipids and may therefore impact the liposome or indeed disrupt it.[17–19] Indeed for liposomes, enzymatic reactions have been shown to influence membrane fluidity and phase behavior.[20] Because lipid membrane fluidity is a key modulator of liposomal TTA-UC, changes in fluidity pertaining to phospholipase action and its hydrolytic products may be important considerations in the design of liposomal TTA-UC systems for *in-cellulo* or *in vivo* application (Scheme 1). Furthermore, enzymatic alterations to TTA-UC may be an interesting way to build logic-gated TTA-UC, *e.g.* for drug delivery. To our knowledge, these questions have not been explored to date.

Phospholipid degradation is an essential process in phospholipid metabolism that occurs in all living organisms. It plays a structural role, for example, in membrane modelling and also serves in specific signalling pathways.[21,22] Phospholipase enzymes are responsible for phospholipid degradation, and they are found throughout the body as both extracellular and intracellular phospholipases. The latter are prevalent in cell membranes and within the lysosome and endoplasmic reticulum (ER).[23] Phospholipase A_2 (PLA_2) is a sub-group of phospholipase enzymes that specifically catalyze the hydrolysis of the *sn*-2 ester bond in phospholipids, releasing fatty acids such as arachidonic acid (AA) and docosahexaenoic acid (DHA) that on further reaction with oxygenases such as COX, form eicosanoids and docosanoids. These are signalling molecules involved in inflammation, pain, immunity, and cell growth. PLA_2 overexpression has been linked to the development and spread of cancers, including notably gastrointenstinal, colon, breast and prostate cancers.[24–26] Thus, PLA_2 is of significant biomedical interest. The physiological concentration of phospholipase seems to vary with intracellular location and tissue type ranging from nanomolar to 100s of nanomolar in activated tissues.[24–26]

Since PLA_2 degrades the liposomal phospholipids into *sn*-1-ether lysophospholipids, this is expected to alter or perhaps even destroy TTA-UC function in TTA-UC liposomes.[27–33] This is explored in this report for the first time, where we examine the impact of PLA_2 enzymolysis on TTA-UC in a liposomal system and unravel the PLA_2-mediated membrane organization, underlying phospholipase kinetics, and roles of Ca^{2+} and inhibition in the system. We apply an optimised and well characterised TTA-UC liposomal system developed by us in this study. This comprises DOPC liposomes containing an iodinated BODIPY sensitizer and a perylene annihilator at a ratio of 1 : 10 (Fig. S1).[4,5,7] We have described how high fluidity of the DOPC membrane is essential in TTA-UC as efficient diffusion supports collision between the constituents leading to efficient TTA-UC. Moreover, because DOPC is unsaturated and forms homogenous liquid-disordered (L_d) phase liposomes, it is likely to be a particularly vulnerable composition and so serves as a good model system to study phospholipid degradation.

To support our study, we also apply a microcavity-based pore-suspended lipid bilayer (MSLB) as a multimodally accessible analytical tool to directly evaluate the impact of PLA_2 on DOPC membrane fluidity using fluorescence lifetime correlation spectroscopy, fluorescence lifetime imaging, and label-free electrochemical impedance spectroscopy.

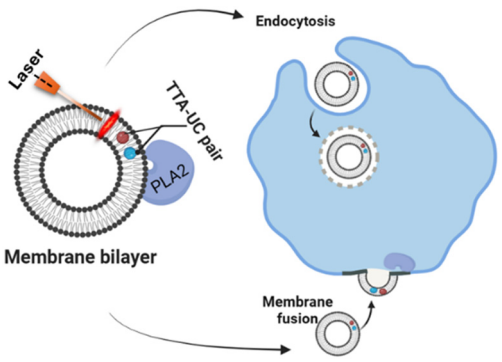

Scheme 1 Schematic illustration of the TTA-UC pair embedded in the liposomal membrane bilayer (left) and the different routes for cell membrane uptake of the nanocarrier. The image was created using BioRender and PowerPoint.

2. Materials and methods

2.1. Materials

Ph-Bodipy-2-perylene-iodine (B2PI; Fig. S1 in the SI) was synthesized according to the protocol described by Reyes *et al.*[4] Perylene and PLA_2 were purchased from Sigma Aldrich. 1,2-Dioleyl-*sn-glycero*-phosphocholine (DOPC) in powder form was purchased from Avanti Polar Lipids. 1,2-Dioleoyl-*sn-glycero*-3-phosphoethanolamine labelled ATTO655 (DOPE-ATTO655) and ATTO532 (DOPE-ATTO532) was purchased from ATTO-TEC GmbH (Siegen, Germany). Polydimethylsiloxane silicon elastomer (PDMS) was purchased from Dow Corning GmbH (Wiesbaden, Germany). Gold disk electrodes consisting of silicon wafers coated

with a 100 nm layer of gold on a 50 Å layer of titanium adhesive were obtained from AMS Biotechnology Inc. Monodisperse polystyrene latex spheres of different sizes were obtained from Bangs Laboratories Inc. The commercial cyanide-free gold plating solution (TG-25 RTU) was obtained from Technic Inc. All other HPLC grade reagents were obtained from Sigma-Aldrich and used as obtained. Ultra-pure water with a resistivity of 18.2 MΩ cm was produced using a Milli-Q (Millipore Academic) system and used for buffer preparation. Tris–HCl buffer was prepared using trisaminomethane, purchased from Sigma-Aldrich to a final concentration of 0.1 M and the pH was adjusted to 7.4 using HCl. 0.1 M NaCl was also added, and the buffer was stored under refrigerated conditions.

2.2. Fabrication of gold and PDMS microcavity arrays

Polystyrene (PS) microsphere lithography was used to fabricate both gold and PDMS microcavity array electrodes, as reported previously.[31–33] A detailed preparation method is given in the SI.

2.3. Liposome preparation

Large unilamellar vesicles (LUV) or liposomes were prepared by the hydration extrusion method.[34,35] The DOPC lipid dissolved in chloroform was mixed with the desired concentrations of the photosensitizer and annihilator or with 0.01% DOPE-ATTO655, in a 1.5 mL vial. The solvent was evaporated under N_2 flow, followed by further drying of the reaction vial *in vacuo* for 30–60 minutes. The resulting thin lipid film was hydrated with 1 mL of Tris–HCl buffer followed by 60 s of vortexing to mix the solution thoroughly. The solution was extruded through a polycarbonate membrane with a 100 nm pore size a minimum of 11 times. The hydrodynamic diameter of the resulting liposomes was measured by dynamic light scattering using a Malvern Zetasizer Ultra instrument. The vesicle solutions were stored at 2 °C and used within 3 weeks of preparation.

2.4. Fabrication of microcavity suspended lipid bilayers

The assembly of the lipid bilayer spanned across the aqueous-filled microcavity array, and both the gold and PDMS array substrates were completed as described previously and explained in the SI using a combination of the Langmuir–Blodgett transfer followed by vesicle fusion (LB-VF) method.

2.5. TTA-UC measurements

The TTA-UC measurements were carried out using a Varian Cary Eclipse fluorescence spectrophotometer using a 532 nm diode laser of 10 mW power (Edmund Optics) as the excitation source with a 1 mm diameter beam and a power density of 1.27 W cm^{-2}. The TTA-UC measurements were performed by blocking the excitation line in bioluminescence measurement mode. The upconverted emission measurements in liposomes were carried out by N_2 purging the sample in a quartz cuvette of 1 cm path length. Upconversion quantum yield and threshold power density measurements were carried out using an Edinburgh Instruments FS5 spectrofluorometer, as previously reported.[14] To activate the enzyme, calcium chloride dihydrate was added to the liposome solution and incubated for 15 minutes. The upconverted emission was recorded over the 400 to 500 nm range to avoid interference from the excitation source.

2.6. Electrochemical impedance spectroscopy

Electrochemical measurements were performed with a CH760A potentiostat (CH Instruments, USA). A standard 3-electrode cell was used, composed of a gold microcavity-suspended bilayer as the working electrode, an Ag/AgCl (1 M KCl) reference electrode and a platinum wire auxiliary electrode. The EIS data were measured over a frequency range of 0.05 to 10^5 Hz with an AC modulation amplitude of 0.01 V at a potential DC bias of 0 V (*vs.* Ag/AgCl). All measurements were carried out in a glass cell (an approximate volume of 4 mL) in contact with Tris–HCl buffer maintained at pH 7.4. EIS of the aqueous-filled microcavity array coated with the lipid bilayer was measured initially prior to the addition of PLA_2 to ensure signal stability upon initial contact with the electrochemical cell/Tris–HCl buffer. At 0 V, an initial fluctuation of resistance was seen that equilibrated within an hour and then remained unchanged over a prolonged window (24 h). Therefore, an equilibration time of 60–90 min was allowed for all EIS cells following which an additional 30 minutes was allowed for incubation of Ca^{2+} prior to the addition of PLA_2. Each EIS measurement takes approximately 4 min and was carried out at room temperature (22 ± 1 °C). The measured data were analysed using ZView software applying an equivalent circuit fitting model (ECM) that was established and tested previously as a good model for the MSLB.[36] Using this approach, we can estimate membrane resistivity and capacitance values before and after PLA_2 binding. The circuit consists of a parallel combination of solution resistance (R_s) and a capacitor in series with a parallel combination of the constant phase element, CPE (C_{array}) and a cavity resistive element (R_{array}) of the microcavity array, and the membrane is approximated by a resistive element (R_M) in parallel with a CPE (Q_M). A constant phase element (CPE) is used in the equivalent circuit instead of pure capacitors, as the impedance of solid electrodes usually deviates from that of a pure capacitor due to microscopic chemical inhomogeneity on both the electrode surface and in the lipid bilayer. Depending on the composition, as described below, from EIS, the bilayer resistance for an intact bilayer ranges from 2 to 10 MΩ (compared to the kΩ resistance of the SAM modified cavity array prior to bilayer deposition). We have previously shown that this resistance range corresponds to an intact SLB and so used the resistance values to validate the bilayer prior to measurement.[37]

2.7. Fluorescence lifetime imaging and fluorescence lifetime correlation spectroscopy

Fluorescence lifetime imaging (FLIM) and fluorescence lifetime correlation spectroscopy (FLCS) experiments were performed using a MicroTime 200 system (PicoQuant GmbH, Germany) consisting of an FCS module, dual SPD detection unit, time-correlated single photon counting (TCSPC), and an inverted Olympus X1-71 microscope equipped with an Olympus UPlan SApo 60×/1.2 water immersion objective. Before FLIM, reflectance

images were collected using an optical density (OD3) filter that assesses the buffer-filled cavities. The fluorescently labelled lipid probe DOPE-ATTO655 was excited using a pulsed picosecond laser at 640 nm (LDH-P-C-640B). A single mode optical fibre guides the laser to the main unit and provides a homogeneous Gaussian profile. The laser was pulsed at 20 MHz, corresponding to an interval of 50 ns. The emitted fluorescence was collected through the same microscope objective; the back scattered light was blocked with a dichroic mirror Z532/635rpc and an HQ670lp AHF/Chroma filter was used to clean up the signal under 640 nm. Fluorescence was detected using a single photon avalanche diode from MPD (PicoQuant). The TCSPC system (PicoHarp 300 from PicoQuant) enabled simultaneous assessment of the lifetime in a nanosecond range along with the time of diffusion in the millisecond range. A 50 μm pinhole was used to confine the volume of detection in the axial direction whilst blocking all off-focal-plane light.

Spatially resolved, point fluorescence lifetime correlation spectroscopy measurements were carried out at microcavity-supported lipid bilayer (MSLB) membranes, supported across porous PDMS substrates, according to a method previously described.[38,39] Measurements were collected focussing on the membrane suspended across the centre of the cavities. The upper leaflet of the bilayer was doped with 0.01 mol% of the fluorescent label DOPE-ATTO655. Point FLCS measurements were then recorded for 30 s per cavity, with an average of 40–50 cavities for each autocorrelation function (ACF) for each bilayer and enzyme type. All measurements were recorded at room temperature (20 ± 0.4 °C). The fluorescence fluctuation intensity is multiplied by a time-shifted replica of varying values (lag time, τ) and the temporal average yields the ACF, $G(\tau)$ for the respective lag time. The ACF obtained from the bilayer spanned over the 2D PDMS array is fitted using eqn (1).

$$G_{2D}(\tau) = \frac{1}{N}\sum_{i=1}^{m}\left(1+\left(\frac{\tau}{\tau_{Di}}\right)^{\alpha}\right)^{-1} \quad (1)$$

where τ_{Di} is the translational transit time of the i-th fluorescent diffusing species in and out of the confocal volume and α is the anomalous coefficient, which deviates from 1 if the diffusion does not follow normal Brownian motion. From the transit time, the diffusion coefficient (D) was determined using eqn (2),

$$D = \frac{\omega^2}{4\tau_D} \quad (2)$$

where ω is the waist diameter of the confocal beam determined to be $1/e^2$ of 0.135 and obtained by calibrating the microscope system with an aqueous solution of ATTO655 with a known diffusion coefficient value diffusing freely in 3D.

3. Results and discussion

3.1. TTA-UC results

To understand the impact, if any, phospholipase A_2 (PLA_2) enzymatic hydrolysis has on TTA-UC efficiency in a liposomal formulation, we used a recently established liposomal TTA-UC system. This system comprises of 0.5 μM B2PI and 5 μM perylene as the TTA-UC pair within DOPC liposomes. This sensitizer-annhilator composition was previously optimised and upon 532 nm laser excitation yields a strong anti-Stokes emission due to perylene with peaks at 444 nm and 474 nm (Fig. S2a, SI).[4,5,7] In our previous report, TTA-UC at DOPC liposome was studied in PBS. In the present study, since PLA_2 enzymatic activity is dependent on the presence of Ca^{2+}, we used Tris–HCl (pH 7.4) buffer to avoid Ca^{2+} complex formation with phosphate anions in the buffer. Ca^{2+} is soluble and stable in Tris–HCl.

Control experiments were first performed to establish if Ca^{2+} ions influence TTA-UC in the liposomes. In the presence of 5 mM Ca^{2+}, no statistically significant impact on the upconversion quantum yield (QY) of the system was observed (Fig. 1a). Upconversion intensity increased modestly, however, by about 10% (Fig. S2a, red (SI)) compared to liposomes in buffer alone (black, Fig. S2a (SI)). Ca^{2+} is thought to preferentially associate with the negatively charged phosphate groups in the membrane headgroup region. This interaction leads to ion–lipid–ion bridges that dehydrate the bilayer surface headgroup through a water squeeze-out mechanism, which likely accounts for the small increase in UC intensity observed.[40]

Next, 5 μM PLA_2 was added to the liposome solution and TTA-UC QY measured at time intervals of 10, 30 and 60 min. In mammalian cells, PLA_2 is usually present in low nanomolar concentrations under normal physiological conditions but during active inflamation or cancer progression, these levels can upregulate to hundreds of nanomolar.[24–26] We used 5 μM PLA_2 in these studies as this exceeds the upper end of the physiological range to ensure the response was the most that could be expected in the physiological system.[41] As shown in Fig. 1a, the enzyme action caused a decrease in TTA-UC quantum yield but by 60 min, the changes had stabilised at ~50% with no further change observed over extended studies of 3 hours. The threshold upconversion intensity was measured before and after incubation with PLA_2 (Fig. 1b) and was observed to increase from 22 mW cm^{-2} to 57 mW cm^{-2}. The stability of liposomes under these enzymatic conditions was confirmed by dynamic light scattering, as detailed below.

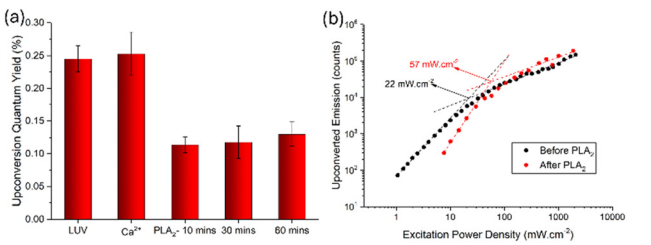

Fig. 1 (a) Upconversion quantum yields from DOPC liposomes incorporated with 0.5 μM B2PI and 5 μM perylene before and after the addition of 5 mM Ca^{2+} and after the subsequent addition of 5 μM PLA_2 measured at 10, 30 and 60 minutes (N = 3). (b) Threshold upconversion intensities before and after addition of PLA_2. All liposomes are in a deaerated Tris–HCl buffer of pH 7.4 and all TTA-UC experiments are carried out in the presence of 20 mM sodium sulphite as an O_2 quencher. All samples were excited with a 532 nm CW laser.

Given the water insolubility of the sensitizer and annihilator, it is very unlikely that dye expulsion is the cause for the observed TTA-UC decrease. Rather, the hydrolysis of PLA_2 is believed to modify the packing of lysophospholipids and the fatty acid catalytic product of DOPC. This is expected to influence the lipid mobility and also phase behaviour, potentially altering both the upconversion quantum yield and threshold power intensity. To investigate this, we determined the diffusion coefficient of the lipids in relation to enzyme treatment in the next section (*vide infra*).

We also confirmed that the changes to TTA-UC are not due to PLA_2 interactions with the membrane in the absence of enzyme activity. To that end, the upconversion emission was measured in the presence of PLA_2 (5 μM) but in the absence of Ca^{2+}. Under these conditions, the TTA-UC intensity did not change, indicating that enzyme hydrolysis is responsible for TTA-UC reduction (Fig. S2b, SI). This observation also adds to the growing body of evidence that Ca^{2+} is necessary for PLA_2 catalytic activity.[42,43]

We then investigated the effect of imipramine, a small-molecule inhibitor of PLA_2, on TTA-UC. After incubating 20 μM of imipramine with 5μM of PLA_2, the solution was added to the liposomal solution containing Ca^{2+}. Fig. 2a shows representative data revealing that upconversion emission does not diminish when catalytic activity of PLA_2 is blocked. This again indicates that lipid hydrolysis is responsible for TTA-UC modification.

In the presence of the inhibitor, modest increases in upconversion emission intensities are observed over time, although the change is not systematic (Fig. 2b). Such variation is not observed in a control where stable TTA-UC output was observed over time without the addition of any reagent. This change is likely due to the impact of imipramine on the membrane itself, which has been shown previously to modestly increase membrane fluidity. To confirm this we completed a control FLCS experiment applying imipramine to the DOPC bilayer where we did observe a modest, but significant, decrease (12 ± 0.2 μm^2 s^{-1}) in DOPC fluidity (Fig. S9).[39]

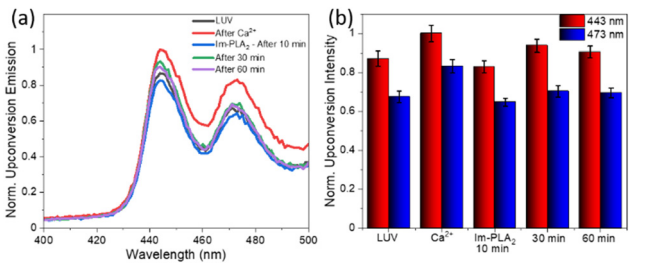

Fig. 2 (a) Normalised TTA-UC emission spectra of DOPC liposomes incorporated with 0.5 μM B2PI and 5 μM perylene before (black) and after (red) the addition of 5 mM Ca^{2+} and after the addition of 5 μM PLA_2 pre-incubated with 20 μM imipramine measured at 10, 30 and 60 minutes. (b) Corresponding intensity histogram for each spectrum in panel (a). All liposomes are suspended in a Tris–HCl buffer of pH 7.4, and measured in triplicate ($N = 3$). All TTA-UC experiments are carried out in the presence of 20 mM sodium sulphite as an O_2 quencher.

3.2. Dynamic light scattering (DLS) studies of PLA_2 action

Dynamic light scattering (DLS) was conducted to determine the effect, if any, that the interaction between PLA_2 and liposomes has on the liposomes' size and integrity. In the absence of PLA_2, the average DOPC liposome diameter containing B2PI and perylene was 120 ± 5 nm in Tris–HCl buffer, pH 7.4 (Fig. S3a, SI). In the absence of Ca^{2+}, the liposome solution remained homogeneous and exhibited an unaltered, unimodal size in the presence of PLA_2 (Fig. S3b, SI). However, after PLA_2 treatment in the presence of Ca^{2+}, the particle size distribution becomes bimodal. As shown in Fig. S3c (SI), the liposomes with a diameter of 120 ± 5 nm remain, but in addition, a new species with an average diameter of 760 nm appears, and the solution becomes somewhat turbid. Although the size dispersity, reflected in the full width at half maximum (FWHM) of the size distribution was found to become narrower on PLA_2 activity as compared to when there is no activity of PLA_2. Conversely, the particle size distribution of liposomes in contact with Ca^{2+} and PLA_2 that has been previously treated with imipramine also (Fig. S3d, SI) remains unchanged with a diameter of 120 ± 5 nm. It has been shown across multiple studies on enzyme responsive liposomes in drug delivery, that enzyme treatment causes an increase in liposome diameter as measured in DLS and alters size distributions of products. This has been attributed to changes in the lipid packing and also liposome fusion induced by lipid hydrolysis, leading to liposome aggregation.[44–46] Our data are strongly consistent with these reports, including the magnitude of the dimension changes that we observe.

Next, to understand the impact of PLA_2 on DOPC membrane properties. We conducted analysis using microcavity-supported lipid bilayers (MSLBs), a true lipid bilayer model membrane suitable for multimodal surface-sensitive interrogation, not accessible to liposomes. We employed single-molecule fluorescence lifetime imaging, fluorescence correlation spectroscopy, and electrochemical impedance to elucidate PLA_2's effects on the DOPC membrane.

3.3. Fluorescence lifetime imaging (FLIM) and fluorescence lifetime correlation spectroscopy (FLCS) studies on PLA_2-catalysed hydrolysis of the DOPC membrane

The decrease in TTA-UC intensity on PLA_2-induced lipid hydrolysis is likely due to changes in the packing order of the membrane. Presumably, this occurs rather than complete membrane disruption since the latter would be expected to extinguish TTA-UC. To confirm this hypothesis, we examined the impact of PLA_2 on membrane properties using fluorescence lifetime imaging (FLIM) and fluorescence lifetime correlation spectroscopy (FLCS). We used micropore-suspended lipid bilayers (MSLBs) over optically transparent PDMS to model membrane behaviour on PLA_2 hydrolysis, as it allowed us to directly interrogate the impact of PLA_2 catalysis on DOPC membrane organization and diffusivity/viscosity.

Fig. 3a shows representative FLIM images of DOPC MSLB supported over the PDMS microcavity array filled with Tris–HCl buffer. To visualize the bilayer, the upper leaflet of the DOPC bilayer was doped with 0.01 mol% of the fluorescent dye-labelled

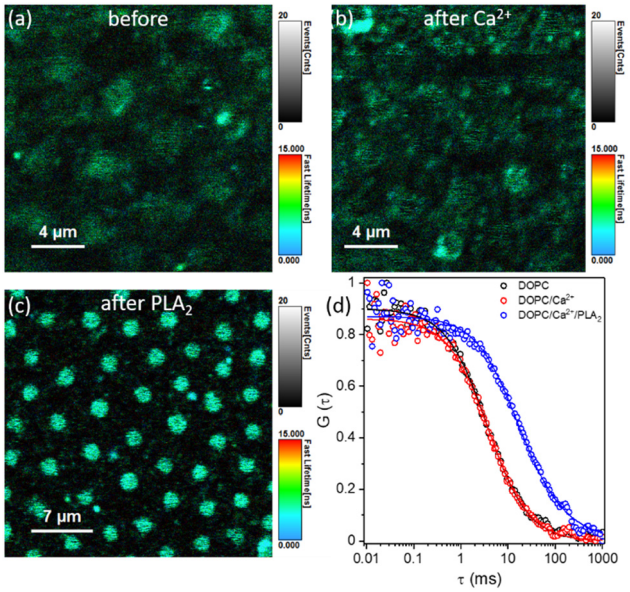

Fig. 3 Fluorescence lifetime images (FLIM) of DOPC MSLBs labelled with 0.01 mol% DOPE-ATTO655 (upper leaflet) (a) before, (b) after the addition of 5 mM Ca^{2+}, and (c) after the addition of 5 μM PLA_2 in the presence of Ca^{2+}. (d) Representative FLCS autocorrelation functions of DOPC MSLBs labelled with 0.01 mol% DOPE-ATTO655 (upper leaflet) before (open black), after 5 mM Ca^{2+} addition (open red) and after the addition of 5 μM PLA_2 in the presence of Ca^{2+} (open blue). FLCS data were collected from 40–50 cavities and the average is shown. The solid lines are the 2D diffusion fit using eqn (1). The scale bar in each panel is 4 μm. All measurements were carried out in Tris–HCl buffer at pH 7.4.

lipid DOPE-ATTO655. The membrane was prepared *via* the Langmuir–Blodgett-vesicle fusion (LB-VF) method, as detailed in the experimental section, and the MSLB was sealed within a microfluidic flow chamber that permits introduction of reagents to the contacting solution at the outer leaflet of the array. Buffer filled cavities, over which the bilayer is spanned, are shown in the reflectance image (Fig. S5a, SI). Upon addition of 5 mM Ca^{2+}, some lateral heterogeneity becomes evident in the FLIM image indicating some reorganization of the membrane (Fig. 3b), notwithstanding the diffraction limit of the method that prevents visualisation of nanoscale reorganisation. Upon addition of PLA_2, the overall molecular brightness increased (Fig. 3c). Fig. 3d shows representative autocorrelation function (ACF) traces for the DOPC bilayer in the absence (open black), in the presence of 5 mM Ca^{2+} (open red), and in the presence of both Ca^{2+} and PLA_2 (open blue). The solid lines in panel 3d show the fit to the 2D diffusion model, as described in eqn (1). All FLCS measurements were performed at the bilayer plane by positioning the FLCS observation volume at the centre of the cavity-spanning bilayer, ensuring that the free-standing bilayer was measured without interference from the solid surface support. The diffusion coefficient of the pore-suspended DOPC bilayer was determined to be 10.1 ± 0.2 $\mu m^2\ s^{-1}$, in agreement with previous reports in both the MLSB and giant unilamellar vesicle (GUV).[47] Upon Ca^{2+} addition, lipid diffusivity reduced to 9.3 ± 0.17 $\mu m^2\ s^{-1}$. Upon further addition of 5 μM PLA_2, post 30 min incubation, the lipid diffusivity reduced dramatically to 1.4 ± 0.3 $\mu m^2\ s^{-1}$. This indicates a marked increase in membrane viscosity upon treatment with the enzyme. In all FLCS experiments both before and after Ca^{2+} and PLA_2 treatment, the anomalous coefficient (α) remained at 1, indicating Brownian diffusion was preserved. To further investigate microviscosity changes of the DOPC bilayer in response to the enzyme, we conducted Laurdan fluorescence spectroscopy in Tris buffer (dotted line) and at DOPC LUVs (black solid line) with and without PLA_2 in the presence of Ca^{2+} (Fig. S4a, SI). The fluorescence spectrum of Laurdan from DOPC LUVs remains virtually the same with the addition of Ca^{2+}. However, in the presence of both Ca^{2+} and PLA_2, there is a notable increase in the fluorescence emission intensity at 430 nm and a corresponding decrease in emission at 490 nm. In the presence of PLA_2, the generalized polarization (GP) value (eqn (S1), SI) significantly increased from −0.18 to −0.07 (Fig. S4b, SI). Thus, consistent with our FCS findings at the MSLB; the Laurdan emission findings indicate that PLA_2/Ca^{2+} enhances membrane ordering/viscosity.

In a control experiment, where PLA_2 was added to the DOPC membrane in the absence of Ca^{2+}, the molecular brightness from FLIM did not change (Fig. S5b and c, SI) compared to that of the FLIM image when Ca^{2+} was present (Fig. 3b and c). Most notably, lipid diffusivity after PLA_2 incubation was reduced modestly to 8.5 ± 0.22 $\mu m^2\ s^{-1}$ as shown in Fig. S5d (red) when Ca^{2+} was not present, in contrast to the dramatic decrease observed when both Ca^{2+} and PLA_2 are present. The lifetime value obtained from the pore-spanning membrane (number of pores analysed = 8) increased barely, from 3.15 ± 0.003 ns to 3.23 ± 0.004 ns (Fig. S6, SI). These relatively minor changes suggest that some physisorption of PLA_2 occurs at the bilayer surface in the absence of Ca^{2+}. However, our data indicate that both Ca^{2+} and PLA_2 must be present to stimulate enzymatic action, and that membrane lipid hydrolysis leads to gross increase in membrane viscosity.[48,49] The fact that the DOPC membrane viscosity increases so significantly during hydrolysis is surprising and suggests that phase changes occur in the membrane, yet there is no fundamental loss of the membrane structural integrity because TTA-UC is retained. The observation is consistent with a report by Leidy *et al.* who showed that DMPC gel-phase membranes underwent a profound phase change during PLA_2 enzymolysis while retaining membrane integrity.[50]

The decrease in TTA-UC we observe is likely due to this reduced lateral diffusivity, which decreases the collision frequency of the annihilator and sensitizer, as reported in more viscous/gel phase lipsosmes, though phase partitioning may also play a role. We saw no evidence, from spectroscopic studies, for loss of the annihilator and sensitizer from the membrane and this is deemed unlikely anyway as they are not water soluble.

We next examined the impact of the PLA_2 inhibitor on membrane organization. Imipramine is an inhibitor of PLA_2 and when the enzyme was pre-treated with this reagent, prior to its incubation with the DOPC MSLB in the presence of Ca^{2+}, the FLIM images (Fig. 4c) were indistinguishable from those of the pristine DOPC MSLB without (Fig. 4a) or with Ca^{2+} (Fig. 4b). Fig. 4d compares ACF traces before (black), after Ca^{2+} (red) and

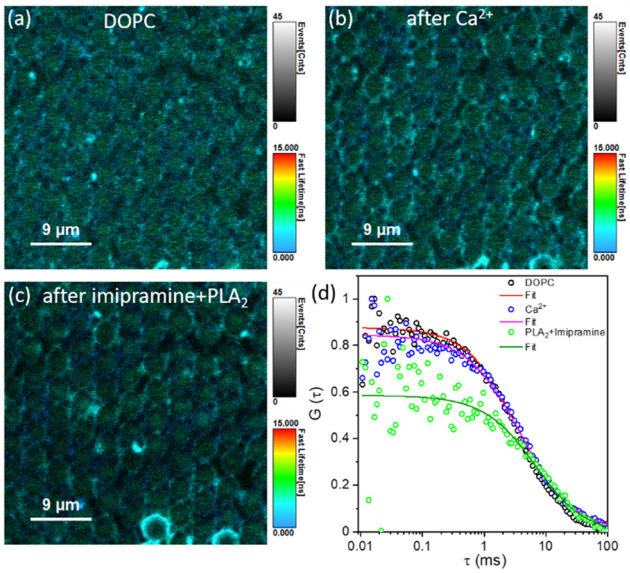

Fig. 4 Fluorescence lifetime images (FLIM) of pristine DOPC MSLBs (a) before and after addition of (b) 5 mM Ca^{2+}, and (c) PLA_2 pre-incubated with imipramine in the presence of Ca^{2+} taken at the identical regime. The concentrations of imipramine and PLA_2 were 20 μM and 5 μM, respectively. In each case in panel b and c, the images were acquired following 30 minutes of incubation. (d) ACF traces obtained from the pristine bilayer (open black) before, after Ca^{2+} (open blue) and after PLA_2-treated imipramine (open green) further spanned over the PDMS microcavity array filled with Tris–HCl buffer. The scale bar in each panel is 9 μm. The solid lines are the 2D diffusion fit using eqn (1).

after imipramine-treated PLA_2 (green) incubation. The membrane diffusivity after 30 min of incubation with PLA_2-treated imipramine is recorded as 4.1 ± 0.3 μm^2 s^{-1}, which is significantly reduced compared to the pristine DOPC membrane. However, the effect is much reduced in comparison to PLA_2 incubation (1.4 ± 0.3 μm^2 s^{-1}). Assuming imipramine is effective as an inhibitor for the hydrolytic action of PLA_2, the resulting viscosity change may be due to the adsorption of imipramine-PLA_2 at the membrane surface, leaving the membrane viscous; such effects have been noted previously on membrane–protein adsorption. This is consistent with our upconversion emission data (*vide infra*). The FLIM images of imipramine treated PLA_2 (Fig. 4c) are also consistent with this model, since they show no evidence of physical changes such as domain formation at the membrane, or any increase in molecular brightness as we observed in the inhibitor free enzyme hydrolysis (*cf.* Fig. 3c). Likewise, the fluorescence lifetime values of labelled lipids in the imipramine/PLA_2 treated membrane did not change when compared to those of the pristine membrane (Fig. S7, SI).

3.4. Electrochemical impedance studies of lipid hydrolysis using PLA_2

Electrochemical impedance of lipid bilayer is highly sensitive to lipid packing, pore formation and membrane remodelling; therefore, we complemented our photophysical studies with electrochemical impedance spectroscopy (EIS) to study PLA_2 action on DOPC membranes. In EIS, the important parameters to consider are membrane resistance and capacitance, which were studied as a function of PLA_2 activity both in the presence and absence of Ca^{2+}, over time. The capacitance characteristics of a lipid bilayer are related to the thickness of the membrane, and non-Faradaic EIS often makes use of alternating current (AC) at different frequencies to evaluate the resistance to ionic conduction through the bilayer. Macromolecular (here PLA_2) binding at the membrane interface can result in thickening of the membrane or an increase in the packing order of the membrane, which is marked by a decrease in capacitance and an increase in resistance; yet, the integrity of the membrane is not compromised. A rise in membrane capacitance with an accompanying resistance decrease, on the other hand, suggests membrane degradation or thinning due to damage or decrease in packing order. In contrast, a decrease in resistance with no change to capacitance is indicative of nanoporation within the membrane.[51,52] These parameters can be derived from the EIS data by fitting with an appropriate equivalent circuit model (ECM). In our EIS experiments, a DOPC bilayer was suspended over a gold microcavity imprinted array, analogous to that used for FLCS studies. This comprised a hexagonally packed microcavity array (1 cm × 1 cm), with a pore diameter of 1 μm and a pore depth of 0.5 μm imprinted array was fabricated over gold-coated silicon chips by a soft-lithography method using 1 μm polystyrene spheres, according to our established protocols.[52–54]

Microcavity suspended lipid bilayers (MSLBs) over the gold microcavity imprinted array were prepared *via* the LB-VF method used for the PDMS arrays. The MSLB serves as the working electrode in a custom-built cell with a volume of 3 to 4 mL. The electrolyte was Tris–buffer, with a pH of 7.4. Typical non-Faradaic Nyquist and angular frequency normalized complex capacitance plots of the bare cavity (black squares) and DOPC MSLB EIS data are shown in Fig. 5 a and b, respectively. The Nyquist traces as semicircle arcs represent

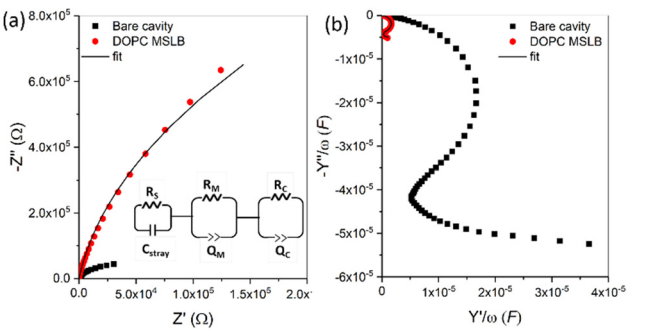

Fig. 5 Representative non-Faradaic (a) Nyquist ($-Z''$ *vs.* Z') and (b) angular frequency normalized complex capacitance ($-Y''/\omega$ *vs.* Y'/ω) plots of bare cavity (black square) and cavity spanned DOPC MSLB (red circle). Inset in panel (a) shows the equivalent circuit model used to fit the EIS data. Solid wine lines in panels (a) and (b) are the corresponding fits. All EIS measurements are performed in Tris–HCl of pH 7.4 buffer at 0 V bias potential with an A.C amplitude of 10 mV within a frequency range of 0.05 Hz and 10^5 Hz. EIS was recorded in a conventional 3-electrode system where the MSLB over gold behaves as the working electrode, Ag/AgCl (1 M KCl) as the reference electrode and Pt wire as the counter electrode.

the real (Z') and imaginary (Z'') parts of the complex impedance, that originate from the resistance and capacitance of the electrochemical cell. When compared to the bare cavity or bilayer-free electrodes (black squares, Fig. 5a), the non-Faradaic Nyquist trace of a DOPC spanned MSLB (red circles) shifts towards $-Z''$ (y-axis), indicating an increase in impedance of the membrane due to the presence of dielectrics (here the lipid bilayer membrane). It is worth noting that the presence of a mercaptohexanethiol SAM only slightly increases the impedance compared to the bare cavity array, because the thiol molecules are spatially restricted to the pore interstitial regions on the top surface of the array. The angular frequency normalized complex capacitance plots ($-Y''/\omega$ *vs.* Y'/ω, where Y is the electrode admittance and ω is the angular frequency) can provide a direct visualization of membrane capacitance properties. Typically, the complex capacitance plots (Fig. 5b) are semi-circular and indicate near-ideal behaviour for the DOPC MSLB. The diameter of the high-frequency semicircle on the imaginary axis is proportional to the magnitude of the bilayer capacitance. As seen from Fig. 5b, the capacitance of a bare gold array electrode (black squares) decreases by one-fold *i.e.*, from 4.2×10^{-5} F to 4×10^{-6} F upon bilayer assembly (red circles), indicating, consistency with previous reports on the pore-supported DOPC membrane.[38] For quantitative analysis, the best fits to the experimental curves are obtained using the equivalent circuit model (ECM) shown in the inset of Fig. 5a. Representative fitted data to Nyquist and complex capacitance plots corresponding to the DOPC bilayer are shown in solid black lines in both panels of Fig. 5a and b.

The absolute magnitude of the DOPC membrane resistance (R_M) and capacitance (Q_M) were measured as 4.7 MΩ and 4.8 μF s^{m-1}, respectively. Note that these values are not normalized to the electroactive area of the working electrode. Also, in the ECM circuit, the introduction of a constant phase element (CPE = $1/Q(j\omega)^m$) rather than a pure capacitor element yields the best fit; where Q is analogous to the magnitude of the capacitance (C), ω is the angular frequency expressed in rad s^{-1}, and m is a CPE exponent real number ($\sim 0.94 \pm 0.01$). While the expression $C_M(\omega) = Q_M\omega^{m-1}$ can be used to estimate true membrane capacitance (C_M) from the Q_M value, it only holds true for a specific ω, limited to the specific ECM, and thus is not used in this work. Nonetheless, when normalized to the actual electroactive surface area, the absolute membrane resistance (R_M) and capacitance (C_M) were found to be in the ranges of 15–40 MΩ cm^2 and 0.7–0.9 μF cm^{-2}, respectively. These values are as expected for a highly insulating defect-free bilayer and range within previously reported values.[38,55–58] We employ here the relative change in membrane resistance (ΔR) and membrane capacitance (ΔQ) values induced by PLA_2 binding to the membrane, as the absolute values vary depending on the electrode area and uniformity of pore packing. ΔR is defined as $R_M^{PLA_2} - R_M^0$, where $R_M^{PLA_2}$ and R_M^0 are the membrane resistances in the presence and absence of PLA_2. Likewise, ΔQ is defined as $Q_M^{PLA_2} - Q_M^0$.

Fig. 6a and b show temporal evolution of the relative resistance and capacitance of DOPC MSLBs induced by PLA_2 in the absence and presence of 5 mM Ca^{2+}, respectively. Prior to

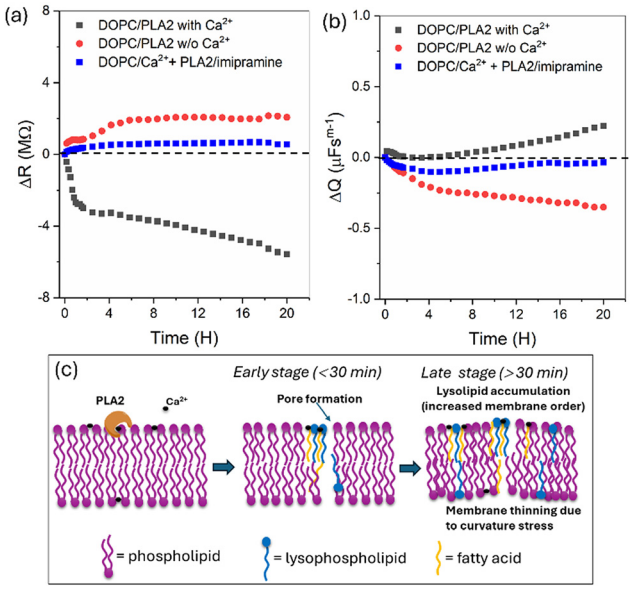

Fig. 6 PLA_2-induced relative change in membrane (a) resistance and (b) capacitance of DOPC MSLBs in the absence (red circles) and presence (black squares) of 5 mM Ca^{2+} in the contact Tris–HCl buffer. The blue data in both panels are the trends in resistance and capacitance changes of DOPC MSLBs induced by pre-incubated 5 μM PLA_2 with 20 μM imipramine. All data points are the average of triplicate measurements under identical experimental conditions. (c) Schematic of the mechanistic view of nanoporation and an increase in membrane order as a result of phospholipid hydrolysis by PLA_2.

PLA_2, the relative change in membrane resistance and capacitance over a 20 h experimental window is stable, as indicated by the horizontal dotted line near to the origin of y-axes of Fig. 6a and b. Without Ca^{2+}, upon addition of PLA_2, the membrane resistance increases and stabilizes within 4–6 hours (red filled circles, Fig. 6a). Correspondingly, capacitance decreases and saturates out within the same time window, (Fig. 6b). Since capacitance (C) is inversely related to the thickness (d) of the bilayer membrane, according to eqn (3),

$$C = \varepsilon\varepsilon_0 A/d \quad (3)$$

where ε is the vacuum permittivity, ε_0 is the dielectric constant and A is the electrode area over which the bilayer is spanned. This suggests membrane thickening, likely due to PLA_2 adsorption to the bilayer. In the presence of 5 mM Ca^{2+}, PLA_2 elicited a rapid drop in membrane resistance that stabilised within an 1 h. Beyond this time, a modest but systematic decrease in resistance was evident (black filled squares, Fig. 6a). This is consistent with the findings of Bilewicz *et al.* who observed a decrease in charge transfer resistance of a hybrid tethered dodecanethiol–DPPC:cholesterol bilayer on PLA_2 binding.[59] The corresponding capacitance data showed no change up to 5 h, whereafter, the capacitance increased modestly over time. A decrease in resistance without accompanying changes to capacitance suggests nanopore formation and the subsequent increase in capacitance is taken to be due to membrane thinning, consistent with the study reported by Jenkins *et al.* at a tethered bilayer platform with a complex lipid composition.[60]

Considering the increased membrane viscosity reflected in the FLCS and Laurdan studies described *vide infra*, it was expected that PLA_2 hydrolysis might manifest as increased membrane resistance. However, our real-time EIS experiments, reveal a dynamic response that reflects a more heterogeneous system: At the early stage of enzyme incubation, pore formation dominates, while at later stages extensive membrane organization occurs. We speculate that as the hydrolytic reaction proceeds, the products (lysophospholipids and fatty acids) form more tightly packed structures within the membrane, potentially forming domains, as indicated by FLCS and Laurdan fluorescence data. However, due to the inverted-cone morphology of lysophospholipids compared to the cylindrical structure of phospholipids, the former induces a positive curvature, resulting in membrane thinning (resistance decrease) at later stages, as evident in our EIS data and schematically illustrated in Fig. 6c. Further evidence of nanopore formation within pore-suspended DOPC lipid bilayers was obtained in an analogous PDMS-based MSLB platform using confocal imaging, where a water soluble membrane impermeable dye, pyranine, was introduced into the aqueous filled cavities prior to bilayer assembly and imaged under a confocal microscope (Fig. S8, SI), confirming that the pristine DOPC membrane is intact and impermeable to pyranine. Following addition of PLA_2 in the presence of Ca^{2+}, extensive pyranine leakage was evident, indicating pore formation without the loss of membrane integrity.[61]

Imipramine inhibits the PLA_2 enzymatic effect, as reflected by a modest overall increase in resistance (blue filled squares, Fig. 6a) and a decrease in capacitance (blue filled squares, Fig. 6b) when PLA_2 is pre-incubated with the 20 μM imipramine drug before treatment of DOPC MSLB in Ca^{2+} containing buffer. The pre-incubation with imipramine may either alter PLA_2 conformation or block the catalytic active sites of the PLA_2 enzyme.[62] Our EIS data indicate weak physisorption of PLA_2 to the membrane's surface when PLA_2 is pre-incubated with imipramine, which supports the modest decrease in lipid diffusivity as discussed earlier.

3.5. Atomic force microscopy studies of lipid hydrolysis using PLA_2

To understand topographic changes in the membrane on PLA_2 interaction, in particular to validate pore formation, which is difficult to resolve by fluorescence imaging, atomic force microscopy (AFM) imaging was carried out on the DOPC planar supported lipid bilayer (SLB) membrane, in this case, over a freshly cleaved mica substrate under buffer.

We selected the SLB for the AFM research rather than the MSLB as the atomically smooth solid support facilitates resolution of nanoscale changes caused by protein binding.[53] The DOPC membrane as assembled on mica is homogeneous (Fig. 7a) as reflected in the corresponding line profile analysis in panel 7e (black). Following 1 h incubation with PLA_2 in the absence of Ca^{2+}, the overall membrane remains homogeneous but with the occasional appearance of nano protuberances of 2–3 nm height attributed to nanoclusters of PLA_2 (*cf.* Panel 7e, blue). These results are consistent with the observed decrease

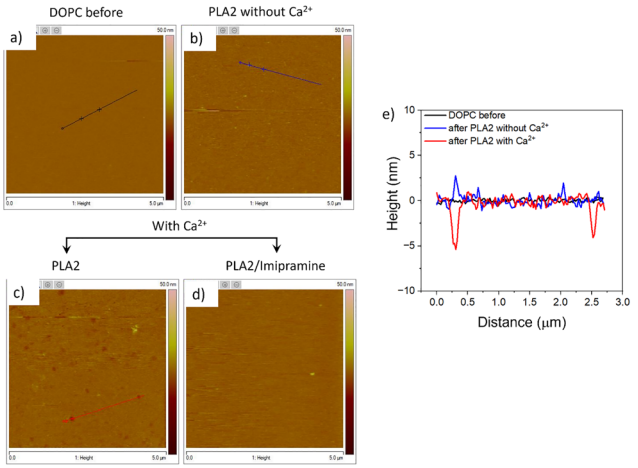

Fig. 7 Topographic AFM images of the DOPC lipid bilayer (a) without and (b) with the presence of PLA_2 in the absence of Ca^{2+} supported over a mica substrate. Panel (c) represents the AFM image of the DOPC bilayer in the presence of 5 mM Ca^{2+} after incubation with PLA_2. Panel (d) represents the AFM image of the DOPC MSLB after incubation of imipramine-treated PLA_2 in the presence of Ca^{2+}. Panel (e) illustrates the line profile analyses obtained from the region of interest as indicated by lines in panels (a–c). All imaging was carried out using Tris–HCl buffer of pH 7.4. The image size was 5 μm × 5 μm.

in membrane admittance seen in EIS data. When Ca^{2+} was present in the buffer, PLA_2 induced significant membrane heterogeneity with extensive changes to lipid packing and pore-like features, as shown in Fig. 7c and the corresponding line profile (red) in Fig. 7e. Again, this is consistent with the impedance data that showed decreased impedance of the membrane, confirming the extensive changes to membrane packing and poration, indicated by FLCS and EIS data, caused by Ca^{2+}-mediated enzymatic action of PLA_2. Also consistent with our earlier observations, when PLA_2 is pre-incubated with imipramine for 30 minutes before incubation with the membrane, the membrane topography remains homogeneous (Fig. 7d), confirming the enzymatic activity of PLA_2 at the membrane is inhibited by imipramine.

4. Conclusions

In conclusion, we investigated the impact of phospholipase enzymatic activity on triplet–triplet annihilation upconversion (TTA-UC) liposomes. We compared TTA-UC from B2PI–perylene reconstituted in DOPC liposomes in the absence and presence of the enzyme phospholipase A_2 (PLA_2) and with and without Ca^{2+}.

Enzymatic hydrolysis of the DOPC liposomal membrane leads to a systematic reduction in TTA-UC intensity as well as QY with an overall ∼50% decrease in light output. Despite this decline, the upconverted emission remains significant, indicating that liposomal TTA-UC function is preserved even during active enzymatic degradation.

The enzymatic action of PLA_2 is dependent on the presence of Ca^{2+} and in the presence of the competitive inhibitor

imipramine, no lipid hydrolysis occurs, and TTA-UC intensity remains indistinguishable from enzyme-free solutions. The decrease in UC intensity is attributed to the impact of enzymatic lipid hydrolysis on the physical properties of the membrane. Our data indicate that it increases lipid packing and decreases membrane fluidity. This is evident from a dramatic reduction in the lipid diffusion coefficient, which decreased from 10.1 ± 0.2 to 1.4 ± 0.3 μm^2 s^{-1} upon enzyme-mediated hydrolysis. These changes are attributed to the accumulation of hydrolytic products, specifically lysolipids and fatty acids in the liposome membrane as well as adsorption of the PLA_2 at the membrane interface.

The impact of enzymatic activity was further confirmed using label-free EIS analysis, where Ca^{2+}-mediated PLA_2 activity increases membrane admittance. Conversely in the absence of Ca^{2+}, or in imipramine-treated PLA_2 in the presence of Ca^{2+}, membrane admittance decreases. The decrease in membrane admittance is attributed to PLA_2 physisorption at the membrane surface in the absence of hydrolysis. Enzyme hydrolysis resulted in widespread membrane reorganisation and increased admittance due to poration, facilitating easier ion transfer across the bilayer. This finding was supported by topographic imaging by AFM.

Overall, this study shows that although diminished, TTA-UC remains efficient following phospholipase enzymatic action on DOPC liposomes. The reduction in efficiency is attributed to an increase in viscosity of the membrane that reduces the collision frequency essential between the sensitizer and annihilator. This indicates that liposomal TTA-UC is maintained, although dye partitioning into different phase domains may play a role. Nonetheless, the data confirm that DOPC TA-UC liposomal systems are robust enough for *in vivo* applications and this approach may also provide a vehicle for developing logic-gated TTA-UC systems for targeted drug delivery and high-resolution bioimaging where endogenous enzymes are present. Given that DOPC liposomes exist homogenously in the L_d phase, it is likely that this composition is representative of the most vulnerable liposome formulation; so we believe that observations are likely true more broadly for other liposome compositions but this is something that will be investigated in future studies.

Author contributions

Amrutha Prabhakaran: methodology, formal analysis, writing – review & editing, and investigation. Nirod Kumar Sarangi: conceptualization, methodology, formal analysis, writing – original draft, writing – review & editing, and investigation. Colm Smith: methodology, formal analysis, and writing – review & editing. Ruben Arturo Arellano Reyes: methodology and formal analysis. Tia E. Keyes: resources, methodology, formal analysis, supervision, funding acquisition, and writing – review & editing.

Conflicts of interest

There are no conflicts to declare.

Data availability

The data supporting this article have been included as part of the supplementary information (SI). Supplementary information: experimental methods for substrate fabrication and additional FLIM, FCS and Laurdan fluorescence data. See DOI: https://doi.org/10.1039/d6tb00152a.

The following datasets are available to researchers upon request to the authors: electrochemical impedance data; fluorescence decay data; fluorescence correlation data.

Acknowledgements

The authors acknowledge the European Union's Horizon 2020 research and innovation programme under the Marie Skłodowska-Curie grant agreement no. 813920 (LogicLab) and Taighde Éireann – Research Ireland under Grant No. 12/RC/2289_P2 and 19/FFP/6428.

References

1 T. N. Singh-Rachford and F. N. Castellano, *Coord. Chem. Rev.*, 2010, **254**, 2560–2573.
2 H.-J. Feng, M.-Y. Zhang, L.-H. Jiang, L. Huang and D.-W. Pang, *Acc. Chem. Res.*, 2025, **58**, 3543–3557.
3 C. Ye, L. Zhou, X. Wang and Z. Liang, *Phys. Chem. Chem. Phys.*, 2016, **18**, 10818–10835.
4 R. A. Arellano-Reyes, A. Prabhakaran, R. C. E. Sia, J. Guthmuller, K. K. Jha, T. Yang, B. Dietzek-Ivanšić, V. McKee and T. E. Keyes, *Chem. – Eur. J.*, 2023, **29**, e202300239.
5 A. Prabhakaran, K. K. Jha, R. C. E. Sia, R. A. Arellano Reyes, N. K. Sarangi, M. Kogut, J. Guthmuller, J. Czub, B. Dietzek-Ivanšić and T. E. Keyes, *ACS Appl. Mater. Interfaces*, 2024, **16**, 29324–29337.
6 W. Wu, H. Guo, W. Wu, S. Ji and J. Zhao, *J. Org. Chem.*, 2011, **76**, 7056–7064.
7 K. Kumar Jha, A. Prabhakaran, R. Cane Sia, R. A. Arellano Reyes, N. Kumar Sarangi, T. Yang, K. Kumar, S. Kupfer, J. Guthmuller, T. E. Keyes and B. Dietzek-Ivanšić, *ChemPhotoChem*, 2023, **7**, e202300073.
8 P. Bharmoria, H. Bildirir and K. Moth-Poulsen, *Chem. Soc. Rev.*, 2020, **49**, 6529–6554.
9 K. K. Jha, A. Prabhakaran, C. S. Burke, M. Schulze, U. S. Schubert, T. E. Keyes, M. Jäger and B. D. Ivanšić, *J. Phys. Chem. C*, 2022, **126**, 4057–4066.
10 Y. Hou, Z. Zhou, K. Huang, H. Yang and G. Han, *ChemPhotoChem*, 2018, **2**, 1005–1011.
11 S. Askes, M. Meijer, T. Bouwens, I. Landman and S. Bonnet, *Molecules*, 2016, **21**, 1460.
12 W. Wang, Q. Liu, C. Zhan, A. Barhoumi, T. Yang, R. G. Wylie, P. A. Armstrong and D. S. Kohane, *Nano Lett.*, 2015, **15**, 6332–6338.
13 L. Huang, Y. Zhao, H. Zhang, K. Huang, J. Yang and G. Han, *Angew. Chem.*, 2017, **129**, 14592–14596.
14 A. Prabhakaran, K. K. Jha, R. C. E. Sia, M. Kogut, J. Czub, J. Guthmuller, C. Smith, C. S. Burke, B. Dietzek-Ivanšić and T. E. Keyes, *J. Phys. Chem. B*, 2025, **129**, 6220–6232.

15 S. H. C. Askes, N. L. Mora, R. Harkes, R. I. Koning, B. Koster, T. Schmidt, A. Kros and S. Bonnet, *Chem. Commun.*, 2015, **51**, 9137–9140.
16 M. Poznik, U. Faltermeier, B. Dick and B. König, *RSC Adv.*, 2016, **6**, 41947–41950.
17 H. L. Verrill, N. A. Pickard and H. D. Gruemer, *Clin. Chem.*, 1977, **23**, 2219–2225.
18 M. Shinitzky and P. Henkart, *Int. Rev. Cytol.*, 1979, **60**, 121–147.
19 G. Lenaz, *Biosci. Rep.*, 1987, **7**, 823–837.
20 K. Jørgensen, J. Davidsen and O. G. Mouritsen, *FEBS Lett.*, 2002, **531**, 23–27.
21 Y. Kita, H. Shindou and T. Shimizu, *Biochim. Biophys. Acta, Mol. Cell Biol. Lipids*, 2019, **1864**, 838–845.
22 R. H. Schaloske and E. A. Dennis, *Biochim. Biophys. Acta, Mol. Cell Biol. Lipids*, 2006, **1761**, 1246–1259.
23 E. A. Dennis, J. Cao, Y.-H. Hsu, V. Magrioti and G. Kokotos, *Chem. Rev.*, 2011, **111**, 6130–6185.
24 M. Menschikowski, A. Hagelgans, B. Nacke, C. Jandeck, O. A. Mareninova, L. Asatryan and G. Siegert, *Tumor Biol.*, 2016, **37**, 8097–8105.
25 X. Wang, C.-J. Huang, G.-Z. Yu, J.-J. Wang, R. Wang, Y.-M. Li and Q. Wu, *Hum. Pathol.*, 2013, **44**, 2020–2027.
26 T. Mirtti, V. J. O. Laine, H. Hiekkanen, S. Hurme, O. Rowe, T. J. Nevalainen, M. Kallajoki and K. Alanen, *APMIS*, 2009, **117**, 151–161.
27 T. Andresen, S. Jensen, T. Kaasgaard and K. Jorgensen, *Curr. Drug Delivery*, 2005, **2**, 353–362.
28 T. L. Andresen, J. Davidsen, M. Begtrup, O. G. Mouritsen and K. Jørgensen, *J. Med. Chem.*, 2004, **47**, 1694–1703.
29 H. Kapalatiya, Y. Madav, V. S. Tambe and S. Wairkar, *Drug Delivery Transl. Res.*, 2022, **12**, 1293–1305.
30 H. Alrbyawi, I. Poudel, M. Annaji, R. D. Arnold, A. K. Tiwari and R. J. Babu, *Pharm. Nanotechnol.*, 2022, **10**, 3–23.
31 G. B. Berselli, N. K. Sarangi, A. V. Gimenez, P. V. Murphy and T. E. Keyes, *Chem. Commun.*, 2020, **56**, 11251–11254.
32 A. Roy, N. K. Sarangi, S. Ghosh, A. Prabhakaran and T. E. Keyes, *J. Phys. Chem. Lett.*, 2023, **14**, 3920–3928.
33 A. V. Gimenez, K. W. Kho and T. E. Keyes, *Nanoscale Adv.*, 2020, **2**, 4740–4756.
34 B. Radwan, A. Prabhakaran, S. Rocchetti, E. Matuszyk, T. E. Keyes and M. Baranska, *Microchim. Acta*, 2023, **190**, 332.
35 D. M. Klein, S. Rodríguez-Jiménez, M. E. Hoefnagel, A. Pannwitz, A. Prabhakaran, M. A. Siegler, T. E. Keyes, E. Reisner, A. M. Brouwer and S. Bonnet, *Chem. – Eur. J.*, 2021, **27**, 17203.
36 N. K. Sarangi, A. Stalcup and T. E. Keyes, *ChemElectroChem*, 2020, **7**, 4535–4542.
37 N. K. Sarangi, A. Prabhakaran and T. E. Keyes, *Electroanalysis*, 2020, **32**, 2936–2945.
38 N. K. Sarangi, A. Prabhakaran and T. E. Keyes, *Langmuir*, 2022, **38**, 6411–6424.
39 N. K. Sarangi, A. Prabhakaran, M. Roantree and T. E. Keyes, *Colloids Surf., B*, 2024, **234**, 113688.
40 N. K. Sarangi, N. Ramesh and A. Patnaik, *J. Chem. Phys.*, 2015, **142**, 024702.
41 H. Cai, E. G. Chiorean, M. V. Chiorean, D. K. Rex, B. W. Robb, N. M. Hahn, Z. Liu, P. J. Loehrer, M. L. Harrison and Y. Xu, *PLoS One*, 2013, **8**, e57081.
42 R. M. Kramer and J. D. Sharp, *FEBS Lett.*, 1997, **410**, 49–53.
43 L.-S. Chang, S.-R. Lin and C.-C. Chang, *J. Protein Chem.*, 1996, **15**, 701–707.
44 X. Zhang, D. S. Alves, J. Lou, S. D. Hill, F. N. Barrera and M. D. Best, *Chem. Commun.*, 2018, **54**, 6169–6172.
45 M. N. Holme, M. H. Rashid, M. R. Thomas, H. M. G. Barriga, K. Herpoldt, R. K. Heenan, C. A. Dreiss, J. L. Bañuelos, H. Xie, I. Yarovsky and M. M. Stevens, *ACS Cent. Sci.*, 2018, **4**, 1023–1030.
46 J. Lou and M. D. Best, *Chem. – Eur. J.*, 2020, **26**, 8597–8607.
47 S. Ramadurai, N. K. Sarangi, S. Maher, N. MacConnell, A. M. Bond, D. McDaid, D. Flynn and T. E. Keyes, *Langmuir*, 2019, **35**, 8095–8109.
48 J. H. Evans, S. H. Gerber, D. Murray and C. C. Leslie, *Mol. Biol. Cell*, 2004, **15**, 371–383.
49 M. S. Hixon, A. Ball and M. H. Gelb, *Biochemistry*, 1998, **37**, 8516–8526.
50 C. Leidy, J. Ocampo, L. Duelund, O. G. Mouritsen, K. Jørgensen and G. H. Peters, *Biophys. J.*, 2011, **101**, 90–99.
51 N. K. Sarangi, S. Mondal and T. E. Keyes, *Biophys. Chem.*, 2025, **322**, 107441.
52 J. Robinson, N. K. Sarangi and T. E. Keyes, *Phys. Chem. Chem. Phys.*, 2023, **25**, 7648–7661.
53 N. K. Sarangi, M. Shafaq-Zadah, G. B. Berselli, J. Robinson, E. Dransart, A. Di Cicco, D. Lévy, L. Johannes and T. E. Keyes, *J. Phys. Chem. B*, 2022, **126**, 10000–10017.
54 A. Roy, S. Byrne, N. K. Sarangi, P. V. Murphy and T. E. Keyes, *Front. Mol. Biosci.*, 2022, **9**, 1017338.
55 G. Wiegand, N. Arribas-Layton, H. Hillebrandt, E. Sackmann and P. Wagner, *J. Phys. Chem. B*, 2002, **106**, 4245–4254.
56 F. Abbasi, J. J. Leitch, Z. Su, G. Szymanski and J. Lipkowski, *Electrochim. Acta*, 2018, **267**, 195–205.
57 M. S. Khan, N. S. Dosoky, B. K. Berdiev and J. D. Williams, *Eur. Biophys. J.*, 2016, **45**, 843–852.
58 P. C. Gufler, D. Pum, U. B. Sleytr and B. Schuster, *Biochim. Biophys. Acta, Biomembr.*, 2004, **1661**, 154–165.
59 A. Więckowska, E. Jabłonowska, E. Rogalska and R. Bilewicz, *Phys. Chem. Chem. Phys.*, 2011, **13**, 9716.
60 T. N. Tun and A. T. A. Jenkins, *Electrochem. Commun.*, 2010, **12**, 1411–1415.
61 R. Georgieva, K. Mircheva, V. Vitkova, K. Balashev, T. Ivanova, C. Tessier, K. Koumanov, P. Nuss, A. Momchilova and G. Staneva, *Langmuir*, 2016, **32**, 1756–1770.
62 K. Kucia, A. Małecki, B. Gabryel and H. I. Trzeciak, *Pol. J. Pharmacol.*, 2003, **55**, 5–15.